Design and material growth of AlGaN-channel two-dimensional-electron gas heterostructures employing strain-controlled quaternary AlGaInN barrier layers

Daiki Hosomi[1]*, Heng Chen[1], Takashi Egawa[1,2], and Makoto Miyoshi[1,2]

[1]*Research Center for Nano Device and System, Nagoya Institute of Technology, Nagoya 466-8555, Japan*

[2]*Innovation Center for Multi-Business of Nitride Semiconductors, Nagoya Institute of Technology, Nagoya 466-8555, Japan*

*E-mail: d.hosomi.904@nitech.jp

In order to improve the thermal stability and ohmic contact resistance in AlGaN-channel two-dimensional electron gas heterostructures, we newly designed strain-controlled quaternary AlGaInN barrier layers, and then we grew them by metalorganic chemical vapor deposition. A 2DEG density as high as 2.5 × 10^{13} cm^{-2} and a good surface morphology were obtained for an $(Al_{0.64}Ga_{0.36})_{0.976}In_{0.024}N/Al_{0.19}Ga_{0.81}N$ heterostructure, in which in-plane tensile strain in the barrier layer was estimated to be 0.51%. It was also confirmed that the $(Al_{0.64}Ga_{0.36})_{0.976}In_{0.024}N/Al_{0.19}Ga_{0.81}N$ heterostructure showed an excellent thermal stability in its 2DEG properties even at high temperatures up to 900°C. As a result of a high temperature treatment, the contact resistance was drastically improved to be 10.5 Ωmm. Although this value is still high, we believe that there is a room to be improved by combining some technique such as the in-situ or ex-situ impurity doping.

Introduction

Heterostructure field-effect transistors (HFETs) utilizing two-dimensional electron gases (2DEGs) caused in, for example, AlGaN/GaN or AlInN/GaN heterointerfaces have been viewed as a promising candidate for next generation high-power/high-frequency electronic devices.[1-3] In addition to conventional GaN-channel heterostructures, AlGaN-channel heterostructures have also been attracting much attention due to their extremely high breakdown voltages[4-10] and less temperature dependence compared to conventional GaN-channel heterostructures.[11-17] Our research group have also reported research results on AlGaN-channel heterostructures and HFETs for the past few years. First, a nearly lattice-matched AlInN/AlGaN heterostructure was grown by metalorganic chemical vapor deposition (MOCVD), and it showed a high 2DEG density of greater than 2.5×10^{13} cm^{-2}.[18] Then, their 2DEG mobility was theoretically analyzed, and it was found that there was room for improvement in its heterointerface roughness.[19] Then, it was confirmed that 2DEG mobility for an AlInN/AlGaN heterostructure was improved with an atomically smooth heterointerface.[20] In addition to these, AlInN/AlGaN HFETs were fabricated and their electrical characteristics including off-state breakdown voltages were evaluated. Eventually, our theoretical analyses have predicted that AlGaN-channel HFETs can show higher device performance than in conventional AlGaN/GaN HFETs with an optimized field-plate electrode by achieving an ohmic contact resistance lower than 1×10^{-5} Ωcm^2.[21] Therefore, our first priority for the research on AlGaN-channel HFETs is now put on the improvement in their contact resistance. In order to achieve good ohmic contacts for wide-bandgap nitride heterostructures, a high-temperature annealing (RTA) is indispensable.[22-24] In our recent work, however, it has become clear that a thermal instability of AlInN/AlGaN heterostructures limited their applicable process temperatures and

thereby restricted the improvement in their contact resistance. Thus, we considered that novel barrier structures with high thermal stability are needed to reduce their ohmic contact resistance for AlGaN-channel heterostructures. In this study, we therefore attempted to utilize strain-controlled quaternary AlGaInN barrier layers instead of nearly lattice-matched AlInN barrier layers for AlGaN-channel heterostructures. Because the quaternary AlGaInN layers can be grown at higher temperatures compared to AlInN layers, they are expected to show better thermotolerance.

2. Experimental procedure

Samples were grown by metalorganic chemical vapor deposition (MOCVD), where trimethyl gallium (TMGa), trimethyl aluminum (TMAl), and trimethyl indium (TMIn) were used as group-III sources, and NH_3 was used as a nitrogen source. A 2-in.-diameter AlN/sapphire template, which had a 1-μm-thick epitaxial AlN film on a *c*-face sapphire, was used as an underlying substrate. The typical X-ray rocking curve (XRC) full widths at half maxima (FWHMs) for the epitaxial AlN film were approximately 100 s and 1,500 s for the (0002) and $(10\bar{1}2)$ reflections, respectively. Fig. 1 shows schematic of an AlGaInN/AlGaN 2DEG heterostructure employed in this study. The heterostructure consisted of, from bottom to top, a 2-μm-thick AlGaN channel layer, a 1-nm-thick AlN interfacial layer, and a 25-nm-thick AlGaInN barrier layer. The layer thicknesses were estimated from the growth rate, and their structural characteristics were evaluated by X-ray diffraction (XRD) measurements and atomic force microscopy (AFM). Hall effect measurements based on van-der Pauw method were carried out for evaluating their 2DEG properties, where ohmic contact metals (Ti/Al = 15/60 nm) were formed using electron-beam (EB) evaporation and were then annealed at different temperatures ranging from 550°C and 900°C in a N_2 flow

ambient. Transfer length measurement (TLM) was carried out for investigating contact resistance, where EB-evaporated Ti/Al/Ni/Au (=15/80/12/40 nm) films were used as ohmic contact metals.

3. Results and discussion

3.1. Design concept for quaternary AlGaInN barrier layers

Here, we describe a design concept for quaternary AlGaInN barrier layers yielding high-density 2DEGs even without a large lattice strain. Fig. 2 shows the relationship between polarization-induced sheet charge density ρ/e and in-plane lattice strain ε_{xx} for 2DEG heterostructures employing an $Al_{0.2}Ga_{0.8}N$ channel and quaternary $(Al_xGa_{1-x})_{1-y}In_yN$ barrier layers. We here utilized ρ/e because it determines the great part of 2DEG density in nitride heterostructures. In this figure, black solid lines and open circles represent calculation results for barrier layers with ternary alloy compositions of $y = 0$ ($Al_xGa_{1-x}N$) and of $x = 1$ ($Al_{1-y}In_yN$). Here, the ε_{xx} values were derived by assuming that the barrier layers were 100% coherently grown for the underlying $Al_{0.2}Ga_{0.8}N$ channel layer. The ρ/e values were derived by considering the spontaneous and piezoelectric polarization effects in the heterostructures. The spontaneous polarization charges P_{SP} in the ternary and quaternary alloys were estimated according to their alloy compositions using material constants of binary alloys.[25] The piezoelectric polarization charges P_{PE} were calculated according to an equation[26]

$$P_{PE} = 2\frac{a - a_0}{a_0}\left(e_{31} - e_{33}\frac{C_{31}}{C_{33}}\right), \qquad (1)$$

where e_{31} and e_{33} are piezoelectric constants, C_{31} and C_{33} are elastic stiffness constants, a_0 and a are in-plane lattice constants for free-standing crystals and actual crystals, respectively, and $(a - a_0)/a_0$ corresponds to the in-plane lattice strain ε_{xx}. The material constants for ternary

and quaternary alloys were derived by using those for binary alloys listed in Table I.[25,27] in accordance with their respective composition ratios. In addition, a relaxation rate of 0.9 was applied for the $Al_{0.2}Ga_{0.8}N$ channel layer, taking into account that AlGaN layers are partially-strained for the underlying AlN layers.[18]

As obvious in results for AlGaN barrier layers shown in Fig.2, introduction of a large in-plane tensile strain caused by a large x value in $Al_xGa_{1-x}N$ is necessary for achieving large ρ/e values. However, increased in-plane tensile strains generally tend to cause crystal deterioration or microcracks on their surfaces. In the case of conventional AlGaN/GaN heterostructures, for example, we empirically know that the in-plane tensile strain in barrier layers needs to be less than approximately 0.6% for obtaining the good 2DEG and crystal properties at the same time.[28,29] From this, it seems difficult for AlGaN barrier layers to achieve high ρ/e values exceeding 2×10^{13} cm^{-2} with a good layer quality. On the other hand, AlInN barrier layers can yield a high ρ/e value greater than 2.5×10^{13} cm^{-2} even with no in-plane tensile strain, $y \simeq 0.13$ in $Al_{1-y}In_yN$, owing to their large spontaneous polarization. Therefore, AlInN barrier layers were considered appropriate for lowering sheet resistance of AlGaN-channel heterostructures. Through our past researches, however, it has been difficult to achieve a low contact resistance in AlInN/AlGaN heterostructures. We understand that this is due to not only their wide bandgap nature but rather a thermal instability resulting from their low growth temperatures. Compared to these, strain-controlled AlGaInN barrier layers may overcome the above-described weaknesses in ternary alloy barrier layers.

Red lines and round dots seen in Fig.2 were drawn by assuming quaternary AlGaInN barrier layers with specific alloy compositions. That is, they show calculation examples obtained by varying the InN molar fraction y in $(Al_xGa_{1-x})_{1-y}In_yN$ barrier layers at a constant x

value of 0.65. As seen in the calculation results, the ε_{xx} value can be reduced by incorporating InN component, for example, from approximately 0.91% at y = 0 to 0.59% at y = 0.025. Moreover, the $(Al_{0.65}Ga_{0.35})_{0.975}In_{0.025}N$ barrier layer yields a large ρ/e value of approximately 2.3×10^{13} cm^{-2}, when it is formed on the $Al_{0.2}Ga_{0.8}N$ channel layer. In addition, the low InN molar fraction of y = 0.025 in $(Al_xGa_{1-x})_{1-y}In_yN$ is also promising for improvements in thermal stability. In accordance to the above design concept, we attempted to form the strain-controlled AlGaInN barrier layers on AlGaN channel layers.

3.2. MOCVD growth and characterization of AlGaInN/AlGaN heterostructures

Based on the design concept descried above, we grew AlGaInN/AlGaN heterostructures with different alloy compositions. Figs. 3(a)-3(c) show surface AFM images of the three samples, and Figs. 3(d)-3(f) show the corresponding XRD reciprocal space maps (RSMs) taken around $(10\bar{1}5)$ reflections. The growth temperatures for the barrier layers of the samples seen in Figs. 3(a), 3(b), and 3(c) were 1000°C, 1000°C, and 900°C, respectively. For reference, the growth temperatures for the conventional AlInN barrier layers in our previous work were approximately 800°C. In the XRD-RSMs, Q_x and Q_y correspond to the reciprocal number of the lattice constant a and c, respectively. The XRD-RSMs confirmed that the quaternary AlGaInN barrier layers were almost 100% coherently grown for the underlying AlGaN channel layers for the all samples. For the barrier layer in the sample shown in Figs. 3(a) and 3(d), which was grown without TMIn supply, the alloy composition and the in-plane lattice strain ε_{xx} were determined to be x = 0.64 in ternary $Al_xGa_{1-x}N$ and 1.3%, respectively, from the XRD-RSM. The other two samples were grown by supplying TMIn gases under the same flow rates of TMGa and TMAl as those

shown in Figs. 3(a) and 3(d). By considering $(Al_{0.64}Ga_{0.36})_{1-y}In_yN$ as their alloy compositions, the y and ε_{xx} values were determined to be 0.008 and 0.78% for the sample shown in Figs. 3(b) and 3(e), and 0.024 and 0.51% for the sample shown in Figs. 3(c) and 3(f), respectively. The structural information mentioned above was summarized in Table II.

From Fig. 3, the surface morphologies and their variation for AlGaInN barrier layers seemed to be closer to those for AlGaN layers[29] rather than granular surface morphologies for AlInN barrier layers.[30] Further, it is obvious that the microcracks generated in the barrier layers decreased with the increase in the InN molar fraction. Simultaneously, it was also confirmed that surface smoothness was improved from 1.3 nm up to 0.6 nm in the root-mean-square (RMS) surface roughness. This quality improvement was probably caused by the reduced in-plane tensile strain. Thus, we conclude that the in-plane tensile strain in the AlGaInN barrier layers were intentionally controlled by varying the InN molar fraction, and it resulted in a smooth surface morphology. 2DEG properties of the AlGaInN/AlGaN heterostructures were evaluated by Hall effect measurement, and the results are summarized in Table II with calculated ρ/e values. The measured 2DEG densities did not show large contradiction compared to the calculated ρ/e values. A relative large 2DEG density of 2.5×10^{13} cm^{-2} was achieved for the $(Al_{0.64}Ga_{0.36})_{0.976}In_{0.024}N/Al_{0.19}Ga_{0.81}N$ heterostructure. As shown in Table II, the measured 2DEG mobilities decreased with the increase in in-plane lattice strain ε_{xx}. This is probably because the microcracks generated in barrier layers reached the heterointerfaces resulting in the deterioration of the 2DEG mobilities.[29] Further, the measured sheet resistance was confirmed to be comparable with that for nearly lattice-matched AlInN/AlGaN 2DEG heterostructure we reported before.[18]

In order to confirm its thermal stability, a strain-controlled $(Al_{0.64}Ga_{0.36})_{0.976}In_{0.024}N/Al_{0.19}Ga_{0.81}N$ heterostructure was annealed at different temperatures

in a N_2 flow ambient and their 2DEG properties were repeatedly evaluated by Hall effect measurements. Figs. 4(a) and 4(b) show the annealing temperature dependence of the measured sheet resistance, 2DEG densities, and 2DEG mobilities, respectively, for the $(Al_{0.64}Ga_{0.36})_{0.976}In_{0.024}N/Al_{0.19}Ga_{0.81}N$ heterostructure, the same sample as shown in Figs. 3(c) and (f). For comparison, the results for a nearly lattice-matched $Al_{0.88}In_{0.12}N/Al_{0.21}Ga_{0.79}N$ heterostructure grown in our previous work are also plotted. As seen in these results, it is obvious that 2DEG properties for the AlInN barrier heterostructure drastically deteriorated even at relative low-temperature treatments. In contrast, the strain-controlled AlGaInN barrier heterostructure showed almost-unchanged 2DEG properties in a wide temperature range up to 900°C. As for the annealed samples, moreover, there are observed no conspicuous changes in the alloy compositions or the surface morphologies.

Finally, the contact resistance for the strain-controlled $(Al_{0.64}Ga_{0.36})_{0.976}In_{0.024}N/Al_{0.19}Ga_{0.81}N$ heterostructure was evaluated by TLM technique. The result showed a contact resistance value of 10.5 Ωmm, which corresponds to the specific contact resistivity of 9.5×10^{-4} Ωcm^2. In the case of an AlInN/AlGaN HFET structure we previously reported, the ohmic contact resistance dominated a very large part for the total device resistance. Although its contact resistance was difficult to estimate owing to their non-linear current-voltage characteristics, it was roughly estimated to be higher than 2×10^{-3} Ωcm^2 at lowest.[21] Thus, in comparison with our previous result, it is clear that the strain-controlled $(Al_{0.64}Ga_{0.36})_{0.976}In_{0.024}N$ barrier layers surely contributed to the improvement in contact resistance of AlGaN-channel heterostructures. In future, there is a possibility that further improvements will be achieved by applying the in-situ or ex-situ impurity doping techniques to AlGaInN barrier layers.

4. Conclusions

Based on a design concept for AlGaN-channel 2DEG heterostructures employing strain-controlled quaternary AlGaInN barrier layers, samples were grown by MOCVD and their structural and electrical characteristics were investigated. From the XRD-RSM and AFM measurements, it was confirmed that the increased InN molar fraction in AlGaInN barrier layers contributed to strain reduction and improvement in the surface morphology and roughness. A strain-controlled $(Al_{0.64}Ga_{0.36})_{0.976}In_{0.024}N/Al_{0.19}Ga_{0.81}N$ heterostructure showed a high 2DEG density of 2.5×10^{13} cm^{-2}. Further, its excellent thermal stability was confirmed in 2DEG properties including 2DEG density, 2DEG mobility and sheet resistance. Consequently, the strain-controlled AlGaInN/AlGaN heterostructure exhibited a lowered contact resistance of 10.5 Ωmm.

Acknowledgements

This work was partially supported by JSPS KAKENHI Grant Number JP16K06298.

References

1) T. Kikkawa, M. Kanamura, T. Ohki, K. Imanishi, K. Watanabe, and K. Joshin, ECS Trans. **50**, 323 (2013).

2) T. Egawa, IEDM Tech. Dig., 2012, 27.1.1.

3) U. K. Mishra, P. Parikh, and Y. -F. Wu, Proc. IEEE **90**, 1022 (2002)

4) T. Nanjo, M. Takeuchi, M. Suita, Y. Abe, T. Oishi, Y. Tokuda, and Y. Aoyagi, IEDM Tech. Dig., 2007, p. 397.

5) T. Nanjo, M. Takeuchi, M. Suita, T. Oishi, Y. Abe, Y. Tokuda, and Y. Aoyagi, Appl. Phys. Lett. **92**, 263502 (2008).

6) T. Nanjo, M. Takeuchi, M. Suita, Y. Abe, T. Oishi, Y. Tokuda, and Y. Aoyagi, Appl. Phys. Express **1**, 011101 (2008).

7) J. J. Freedsman, T. Hamada, M. Miyoshi, and T. Egawa, IEEE Electron Device Lett. **38**, 497 (2017).

8) S. Bajaj, F. Akyol, S. Krishnamoorthy, Y. Zhang, and S. Rajan, Appl. Phys. Lett. **109**, 133508 (2016).

9) H. Tokuda, M. Hatano, N. Yafune, S. Hashimoto, K. Akita, Y. Yamamoto, and M. Kuzuhara, Appl. Phys. Express **3**, 121003 (2010).

10) J. Xue, J. Zhang, and Y. Hao, Appl. Phys. Lett. **108**, 013508 (2016).

11) M. Hatano, N. Kunishio, H. Chikaoka, J. Yamazaki, Z. B. Makhzani, N. Yafune, K. Sakuno, S. Hashimoto, K. Akita, Y. Yamamoto, and M. Kuzuhara, IEEE Int. Conf. Compound Semiconductor Manufacturing Technology (CS MANTECH) Dig., 2010, p. 101.

12) M. Hatano, N. Yafune, H. Tokuda, Y. Yamamoto, S. Hashimoto, K. Akita, and M. Kuzuhara, IEICE Trans, Electron. **E95-C**, 1332 (2012).

13) S. Hashimoto, K. Akita, T. Tanabe, H. Nakahata, K. Takeda, and H.Amano, Phys. Status Solidi C **7**, 1938 (2010).

14) S. Hashimoto, K. Akita, Y. Yamamoto, M. Ueno, T. Nakamura, N. Yafune, K. Sakuno, H. Tokuda, M. Kuzuhara, K. Takeda, M. Iwaya, and H. Amano, Phys. Status Solidi C **9**, 373 (2012).

15) J. Liu, Y. Zhou, R. Chu, Y. Cai, K. J. Chen, and K. M. Lau, IEDM Tech. Dig., 2004, p. 811.

16) A. Raman, S. Dasgupta, S. Rajan, J. S. Speck, and U. K. Mishra, Jpn. J. Appl. Phys. **47**, 3359 (2008).

17) J. Liu, Y. Zhou, R. Chu, Y. Cai, K. J. Chen, and K. M. Lau, IEEE Electron Device Lett. **26**, 145 (2005).

18) M. Miyoshi, S. Fujita, and T. Egawa, Appl. Phys. Express **8**, 021001 (2015).

19) M. Miyoshi, S. Fujita, and T. Egawa, Appl. Phys. Express **8**, 051003 (2015).

20) D. Hosomi, Y. Miyachi, T. Egawa, and M. Miyoshi, Jpn. J. Appl. Phys. **57**, 04FG12 (2018).

21) M. Miyoshi, T. Tsutsumi, G. Nishino, Y. Miyachi, M. Okada, J. J. Freedsman, and T.Egawa, J. Vac. Sci. Technol. B **34**, 050602 (2016).

22) A. N. Bright, P. J. Thomas, M. Weyland, D. M. Tricker, C. J. Humphreys, and R. Davies, J. Appl. Phys. **89**, 3143 (2000).

23) M. W. Fay, G. Moldovan, P. D. Brown, I. Harrison, J. C. Birbeck, B. T. Hughes, M. J. Uren, and T. Martin, J. Appl. Phys. **92**, 94 (2002).

24) F. Iucolano, G. Greco, and F. Roccaforte, Appl. Phys. Lett. **103**, 201604 (2013).

25) F. Bernardini, V. Fiorentini, and D. Vanderbilt, Phys. Rev. B **63**, 193201 (2001).

26) O. Ambacher, B. Foutz, J. Smart, J. R. Shealy, N. G. Weimann, K. Chu, M. Murphy, A. J. Sierakowski, W. J. Schaff, L. F. Eastman, R. Dimitrov, A. Mitchell, and M. Stutzmann, J. Appl. Phys. **87**, 334 (2000).

27) M. Shur, M. Shatalov, A. Dobrinsky, and R. Gaska, in GaN and ZnO-Based Materials and Devices, ed. S. Pearton (Springer, Heidelberg, 2012) Springer Series in Materials Science, Vol. 156, p. 83

28) M. Miyoshi, T. Egawa, and H. Ishikawa, J. Vac. Sci. Technol. B **23**, 1527 (2005).

29) M. Miyoshi, M. Sakai, H. Ishikawa, T. Egawa, T. Jimbo, M. Tanaka, and O. Oda, J. Cryst. Growth **272**, 293-299 (2004)

30) M. Miyoshi, Y. Kuraoka, M. Tanaka, and T. Egawa, Appl. Phys. Express **1**, 081102 (2008)

Table I. Physical constants used in this study.[25,27)]

Item	AlN	GaN	InN
Intrinsic lattice constant			
a_0 (Å) [27)]	3.112	3.188	3.54
Elastic stiffness constants			
C_{13} (GPa) [25)]	94	68	70
C_{33} (GPa) [25)]	377	354	205
Spontaneous polarization charge			
P_{SP} (C/m^2) [25)]	-0.09	-0.034	-0.042
Piezoelectric constants			
e_{31} (C/m^2) [25)]	-0.62	-0.37	-0.45
e_{33} (C/m^2) [25)]	1.50	0.67	0.81

Table II. Sample structures, in-plane lattice strain (ε_{xx}) in a barrier layer estimated by XRD-RSMs, and room-temperature 2DEG density N_s, mobility μ, and sheet resistance R_{sh} obtained by Hall effect measurements for the different-alloy-composition AlGaInN/AlGaN heterostructures. Calculated ε_{xx} and ρ/e values are also listed.

Sample structure	ε_{xx} (%)	Calculation		Measured by Hall effect		
		ε_{xx} (%)	ρ/e (cm^{-2})	N_s (cm^{-2})	μ (cm^2/Vs)	R_{sh} (Ω/sq.)
$Al_{0.64}Ga_{0.36}N/Al_{0.15}Ga_{0.85}N$	1.3	1.0	2.9×10^{13}	4.7×10^{13}	129	1028
$(Al_{0.64}Ga_{0.36})_{0.992}In_{0.008}N$ /$Al_{0.17}Ga_{0.83}N$	0.78	0.85	2.6×10^{13}	3.9×10^{13}	172	932
$(Al_{0.64}Ga_{0.36})_{0.976}In_{0.024}N$ /$Al_{0.19}Ga_{0.81}N$	0.51	0.58	2.2×10^{13}	2.5×10^{13}	216	1158

Figure captions

Figure 1. Schematic cross section of an AlGaInN/AlGaN 2DEG heterostructure.

Figure 2. (Color online) The relationship between polarization-induced sheet charge density ρ/e and in-plane lattice strain ε_{xx} for 2DEG heterostructures employing an $Al_{0.2}Ga_{0.8}N$ channel and quaternary $(Al_xGa_{1-x})_{1-y}In_yN$ barrier layers.

Figure 3. (Color online) Surface AFM images with a scanning area of 1 μm × 1 μm for (a) AlGaN/AlGaN heterostructure without InN incorporation, (b) AlGaInN/AlGaN heterostructure with a low InN molar fraction, and (c) AlGaInN/AlGaN heterostructure with a high InN molar fraction. (d), (e) and (f) XRD-RSMs taken around $(10\bar{1}5)$ reflection for the same samples as seen in (a), (b) and (c). The measured root-mean-square (RMS) values are also shown in AFM images. The InN molar fractions y and in-plane lattice strains in $(Al_{0.64}Ga_{0.36})_{1-y}In_yN$ barrier layers are also shown in XRD-RSMs.

Figure 4. (Color online) Annealing temperature dependence of (a) sheet resistance R_{sh}, (b) 2DEG mobility μ and 2DEG density N_s, measured by Hall effect for a strain-controlled $(Al_{0.64}Ga_{0.36})_{0.976}In_{0.024}N/Al_{0.19}Ga_{0.81}N$ heterostructure. For comparison, round dots represented results for a nearly lattice-matched $Al_{0.88}In_{0.12}N/Al_{0.21}Ga_{0.79}N$ heterostructure grown at low temperature of 800°C.

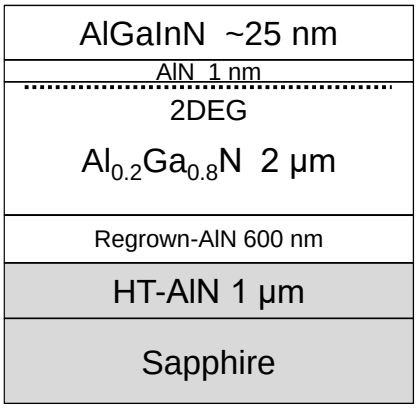
AlGaInN ~25 nm
AlN 1 nm
2DEG
$Al_{0.2}Ga_{0.8}N$ 2 µm
Regrown-AlN 600 nm
HT-AlN 1 µm
Sapphire

Figure 1

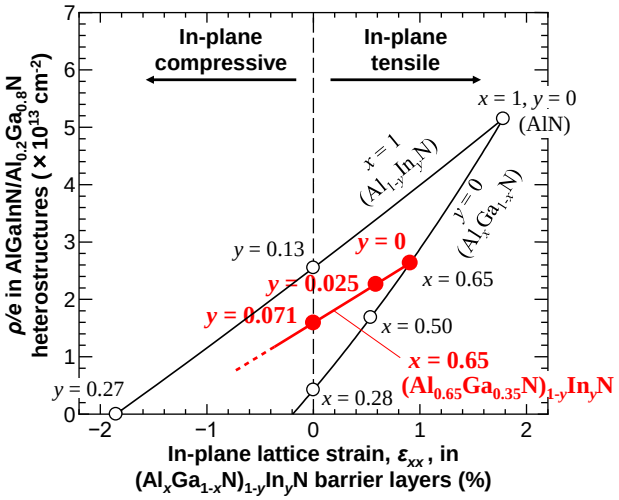
In-plane compressive
In-plane tensile
x = 1, y = 0
(AlN)
x = 1
(Al1-yInyN)
y = 0
(AlxGa1-xN)
y = 0.13
y = 0
y = 0.025
y = 0.071
x = 0.65
x = 0.50
x = 0.65
(Al0.65Ga0.35N)1-yInyN
y = 0.27
x = 0.28
ρ/e in AlGaInN/Al0.2Ga0.8N heterostructures (×10^13 cm^-2)
In-plane lattice strain, εxx, in (AlxGa1-xN)1-yInyN barrier layers (%)

Figure 2

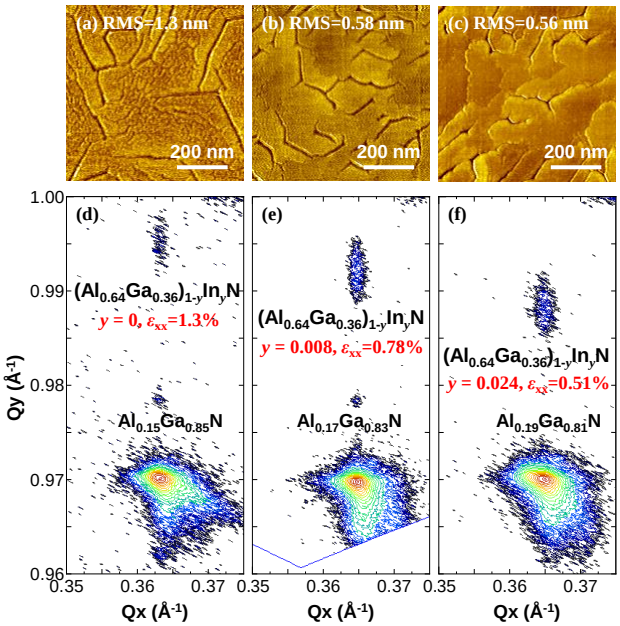
(a) RMS=1.3 nm
200 nm
(b) RMS=0.58 nm
200 nm
(c) RMS=0.56 nm
200 nm
(d)
(Al0.64Ga0.36)1-yInyN
y = 0, εxx=1.3%
Al0.15Ga0.85N
(e)
(Al0.64Ga0.36)1-yInyN
y = 0.008, εxx=0.78%
Al0.17Ga0.83N
(f)
(Al0.64Ga0.36)1-yInyN
y = 0.024, εxx=0.51%
Al0.19Ga0.81N
Qy (Å-1)
1.00
0.99
0.98
0.97
0.96
0.35
0.36
0.37
Qx (Å-1)

Figure 3

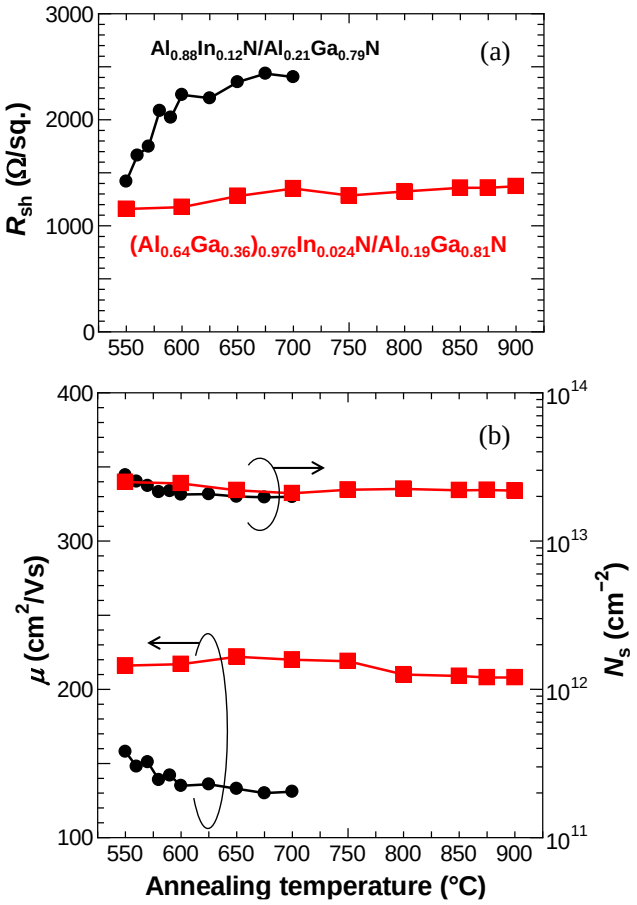
3000
2000
1000
0
R_{sh} (Ω/sq.)
$Al_{0.88}In_{0.12}N/Al_{0.21}Ga_{0.79}N$
(a)
$(Al_{0.64}Ga_{0.36})_{0.976}In_{0.024}N/Al_{0.19}Ga_{0.81}N$
550 600 650 700 750 800 850 900
400
300
200
100
μ (cm^2/Vs)
(b)
10^{14}
10^{13}
10^{12}
10^{11}
N_s (cm^{-2})
550 600 650 700 750 800 850 900
Annealing temperature (°C)

Figure 4